

# FedDyMem: Efficient Federated Learning with Dynamic Memory and Memory-Reduce for Unsupervised Image Anomaly Detection

Silin Chen, Kangjian Di, Yichu Xu, Han-Jia Ye, Wenhan Luo, Ningmu Zou<sup>†</sup>

**Abstract**—Unsupervised image anomaly detection (UAD) has become a critical process in industrial and medical applications, but it faces growing challenges due to increasing concerns over data privacy. The limited class diversity inherent to one-class classification tasks, combined with distribution biases caused by variations in products across and within clients, poses significant challenges for preserving data privacy with federated UAD. Thus, this article proposes an efficient federated learning method with dynamic memory and memory-reduce for unsupervised image anomaly detection, called FedDyMem. Considering all client data belongs to a single class (i.e., normal sample) in UAD and the distribution of intra-class features demonstrates significant skewness, FedDyMem facilitates knowledge sharing between the client and server through the client’s dynamic memory bank instead of model parameters. In the local clients, a memory generator and a metric loss are employed to improve the consistency of the feature distribution for normal samples, leveraging the local model to update the memory bank dynamically. For efficient communication, a memory-reduce method based on weighted averages is proposed to significantly decrease the scale of memory banks. On the server, global memory is constructed and distributed to individual clients through k-means aggregation. Experiments conducted on six industrial and medical datasets, comprising a mixture of six products or health screening types derived from eleven public datasets, demonstrate the effectiveness of FedDyMem.

**Index Terms**—Federated learning, unsupervised anomaly detection, feature distribution shift, communication efficiency, dynamic memory bank.

## I. INTRODUCTION

UNSUPERVISED image anomaly detection has achieved significant success in various domains, such as industrial inspection [1] and medical disease recognition [2]. However, these methods highly depend on the availability of large-scale datasets for centralized training. Industrial companies and healthcare organizations often have practical limitations in collecting and aggregating raw data, which significantly challenges centralized learning approaches [3], [4]. Recently,

<sup>†</sup> corresponding authors.

Silin Chen and Kangjian Di are the School of Integrated Circuits, Nanjing University, Suzhou, China. Email: {silin.chen, kangjiandi}@smail.nju.edu.cn.

Yichu Xu and Han-Jia Ye are with both the National Key Laboratory for Novel Software Technology, Nanjing University, Nanjing, 210023, China and the School of Artificial Intelligence, Nanjing University, Nanjing, 210023, China. Email: {xuyc, yehj}@lamda.nju.edu.cn.

Wenhan Luo is with the Hong Kong University of Science and Technology, Clear Water Bay, Hong Kong. Email: whluo.china@gmail.com.

Ningmu Zou is with both the School of Integrated Circuits, Nanjing University, Suzhou, China and the Interdisciplinary Research Center for Future Intelligent Chips (Chip-X), Nanjing University, Suzhou, China. Email: nzou@nju.edu.cn.

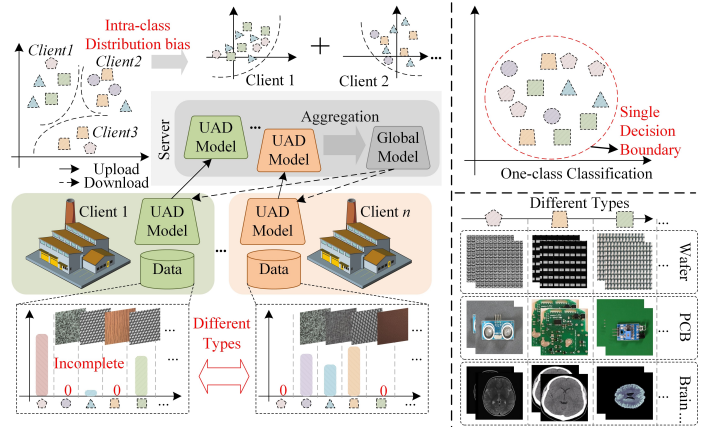


Fig. 1. Illustration of federated learning in UAD. As shown on the left, for the same product anomaly detection, an intra-class distribution bias exists between local models, caused by each client possessing varying and incomplete subsets of product types. As shown in the top right, federated UAD aims to establish a single decision boundary for one-class classification within the global model. Examples of type differences in anomaly detection for different products are shown in the right down.

federated learning has been developed as a privacy-preserving paradigm for machine learning, providing collaborative model training across distributed devices while maintaining raw data locally and not transmitting to central servers [5], [6]. Thus, the integration of local training and global aggregation strategies has garnered significant attention in industrial and healthcare domains, enabling data privacy protection [7]–[9].

Federated learning is applicable to both supervised and unsupervised learning scenarios. Recent developments in unsupervised federated learning have shown significant progress [10]. These methods are often focused on learning a general representation or prototype by self-supervised learning (SSL) while keeping private data decentralized and unlabeled. Some methods continue to rely on local updates and aggregation of model parameters to train a global model for representation generation [11], [12]. Alternatively, other approaches take advantage of representation sharing, using knowledge distillation (KD) to construct a robust representation space [13]–[15]. However, these methods are designed to obtain a more efficient representation by SSL and require local fine-tuning through a supervised linear evaluation protocol [11] following federated learning. Consequently, existing approaches in unsupervised federated learning are inadequate for addressing the UAD task.

With the advancements in UAD using deep learning,

reconstruction-based methods [16]–[18] have emerged as prominent strategies by learning to accurately reconstruct normal samples while minimizing reconstruction loss, thereby enabling the identification of anomalies as deviations from expected reconstructions. Intuitively, integrating reconstruction loss functions to locally optimize the model, followed by aggregating the model weights through federated learning approaches, presents a promising avenue for enabling federated learning in UAD. However, as shown in Fig. 1, the intra-class distribution bias within the normal sample class, caused by variations in products, is also an important issue in UAD [19]. Similarly, data heterogeneity in federated learning can lead to significant performance degradation and convergence challenges, primarily due to inconsistencies in local updates and optimization dynamics [20], [21]. Recently, most of the current federated learning methods focus on addressing the challenges posed by data heterogeneity [22]–[27]. To address the feature shift challenge in federated learning, some methods have proposed incorporating local constraints by the global model or gradient information, thereby mitigating discrepancies across clients [20], [22], [23], [28], [29]. Despite these efforts, the significant intra-class feature distribution bias in UAD results in insufficient global information to effectively capture the representations and knowledge of diverse products [30]. Meanwhile, other researchers have addressed this issue by synthesizing data [31], [32]. However, sharing additional data among clients inherently increases the risk of data privacy leakage [33]. Recent approaches have increasingly emphasized prototype-learning methods to tackle the challenges posed by inconsistent data distributions. These methods construct category-specific global and local prototypes by leveraging feature alignment, effectively addressing generalization gaps across local clients [26], [27], [34], [35]. Nevertheless, reconstruction-based loss functions in UAD often lead to overfitting on local features of normal samples [36]. The use of a single category hinders effective global feature aggregation and prevents normal representations from achieving a compact distribution. As a result, the aggregated prototypes deviate from the desired global distribution of normal samples.

Furthermore, communication between clients in federated learning is limited by network bandwidth, unreliable connections, and varying device statuses. Consequently, designing communication-efficient algorithms is crucial to overcome these challenges [37]. Existing methods primarily tackle this issue by either decreasing the total number of communication rounds required for model convergence or reducing the data uploaded during each communication round [38]. To accelerate global convergence, some approaches leverage mechanisms such as localized model updates [39] and gradient optimization enhancements [40], effectively reducing the number of communication rounds. To reduce the data uploaded, methods such as model compression [41]–[43] and selective client participation [44] have been extensively explored to minimize communication overhead. In this article, we aim to enhance the efficiency of federated learning by minimizing communication overhead through effective data reduction.

To summarize, federated UAD must address the following key challenges: 1) enabling each client to perform end-to-

end unsupervised anomaly detection without the reliance on additional labeled data or supervised fine-tuning, utilizing only one-class (normal) samples as the basis for training. 2) mitigating significant distribution biases in normal sample data across clients, which arise due to the heterogeneous product types or health screening modalities within the federated learning framework. 3) ensuring efficient communication between clients and the central server to minimize overhead. This article introduces FedDyMem, an efficient federated learning framework with dynamic memory and memory-reduce, specifically designed to tackle the aforementioned challenges in federated UAD. FedDyMem facilitates knowledge transfer in federated learning by sharing the memory bank instead of model parameters among clients. Specifically, it constructs a local memory bank using the limited dataset of normal samples available at each client. To address the challenge of intra-class distribution bias in different clients, a memory generator and a metric loss function are introduced to improve the consistency of normal feature distributions. Then the local memory bank is dynamically updated by the local client model before uploading. To mitigate distribution bias during aggregation, FedDyMem employs k-means clustering to extract general distribution from different clients, thereby ensuring effective aggregation without confusion. Considering communication efficiency, a memory-reduce method is proposed to decrease the scale of memory banks during dynamic updates. To construct diverse data for our experiments, we categorize the 11 public datasets into six distinct types based on their inherent characteristics. We then evaluate our proposed method separately on six product or health screening types, achieving state-of-the-art performance in each case. The major contributions of this article are summarized as follows:

- To the best of our knowledge, FedDyMem is the first federated learning framework designed specifically for unsupervised image anomaly detection. This framework facilitates collaborative training using only normal samples available on the client side. To ensure privacy-preserving knowledge sharing, we introduce a dynamic memory bank as an alternative to exchanging model parameters.
- To address the significant distribution biases of normal samples across clients, we incorporate a memory generator and a metric loss function that improve the consistency of feature distributions. Additionally, we employ k-means clustering during the aggregation phase to reduce inter-client discrepancies and mitigate potential ambiguities.
- To improve communication efficiency, we propose a memory-reduce method based on a dynamic weighted average. This method substantially decreases the size of the memory bank, thereby minimizing communication overhead while preserving performance.
- We have collected eleven image anomaly detection datasets from various industrial and medical domains. These datasets are further divided into six datasets depending on the type of product or health screening. Comprehensive experiments demonstrate that FedDyMem achieves excellent federated UAD performance.

## II. RELATED WORK

### A. Unsupervised Image Anomaly Detection

The objective of UAD is to identify whether a given sample is anomalous and to precisely localize the anomaly regions, using a training dataset that comprises only normal samples [1]. The reconstruction-based methods are significant in UAD, which assumes that anomalous samples cannot be accurately reconstructed by feature learning models trained exclusively on normal samples [17], [18], [45]–[48]. In contrast to traditional UAD approaches, which rely on a single, centralized training dataset, federated UAD requires the efficient aggregation of information from samples distributed across multiple clients. Reconstruction-based methods, however, typically rely solely on normal samples within the training set and fail to capture key characteristics of out-of-distribution samples. Another widely utilized approach for anomaly detection is the memory bank-based method. SPADE [49] proposed a semantic pyramid structure to construct a pixel-level feature memory, effectively facilitating anomaly detection. PaDiM [50] employed Gaussian distributions derived from normal samples as the memory bank and utilized the Mahalanobis distance as the anomaly metric. PatchCore [51] introduced local neighborhood aggregation to expand the receptive field of the memory bank while preserving resolution. Additionally, PatchCore implemented a greedy core-set subsampling strategy to reduce the memory bank size without significant performance degradation. PNI [52] further advanced the paradigm by integrating spatial and neighborhood information into the memory bank construction, thereby improving its capacity to represent normal samples comprehensively. These methods extract features from normal images and store them within a feature memory bank. During testing, the sample queries the memory bank to retrieve feature corresponding to the  $k$ -nearest neighbors. However, the memory banks are non-trainable, limiting their capacity to learn information across local clients in the federated learning.

### B. Federated Learning

The federated learning can be divided into supervised-based and unsupervised-based methods. In unsupervised federated learning, most existing methods focused on representation learning or prototype-based learning, which aimed to learn good feature representations from unlabeled data to facilitate downstream machine learning tasks [11]–[15]. However, these methods depend on aligning local representations with global representations, a task that proves challenging for UADs constrained to a single category. ProtoFL [53] was proposed to integrate federated learning with prototyping for addressing one-class classification. However, its two-stage fine-tuning method, which utilizes normalizing flow for representation learning, introduces unnecessary computational overhead and ignores distribution bias among clients in UAD. Furthermore, most unsupervised federated learning approaches require supervised fine-tuning, which limits their applicability to UAD.

FedAvg [54] is a foundational approach in federated learning that enables the training of a global model by aggregating

parameters from locally trained models. Despite its effectiveness, the performance of FedAvg degrades significantly with high data heterogeneity. FedProx [22] and SCAFFOLD [20] demonstrated enhanced performance through a global penalty term, effectively addressing and mitigating discrepancies. Other methods have now been developed to address the data heterogeneity with the personalized model. FedBN [23] mitigates data heterogeneity challenges in federated learning by maintaining BN parameters that are specific to each client’s local model. APPLE [29] aggregates client models locally by learning precise weight updates instead of relying on approximations. Recent approaches address generalization gaps across local clients by leveraging feature alignment to construct category-specific global and local prototypes [26], [27], [34], [35]. Nevertheless, the aforementioned methods face significant challenges in UAD, including high communication overhead, insufficient representation diversity and pronounced intra-class distribution bias.

## III. PRELIMINARY

### A. Typical Federated Learning

In the typical federated learning, such as FedAvg [54], there exist  $N$  clients  $\{\mathcal{C}_n\}_{n=1}^N$  with their individual datasets  $\{\mathcal{D}_n = (\mathcal{X}_n, \mathcal{Y}_n) \sim \mathbb{P}_n(\mathcal{X}, \mathcal{Y})\}_{n=1}^N$  and local models  $\{f^n(\cdot; \mathbf{W}^n): \mathcal{X}_n \rightarrow \mathcal{Y}_n\}_{n=1}^N$ , where  $n$  is the index for the client,  $(\mathcal{X}_n, \mathcal{Y}_n)$  denotes a set of samples and labels on the  $n$ -th client,  $\mathbb{P}_n(\mathcal{X}, \mathcal{Y})$  represent the joint distribution of samples and labels. The objective of the typical federated learning is to facilitate collaborative training of a global model  $\mathbf{W}^G$  that generalizes effectively across the entire dataset  $\mathcal{D}$  while ensuring data privacy. The global training optimization target is:

$$\min_{\mathbf{W}^G} \mathcal{L}(\mathbf{W}^G) \triangleq \sum_{n=1}^N z_n \mathcal{L}_n(\mathbf{W}^n), \quad (1)$$

where the  $z_n$  denotes the weight coefficient which is computed as  $\frac{|\mathcal{D}_n|}{|\mathcal{D}|}$  in FedAvg, where the  $|\mathcal{D}| = \bigcup_{n=1}^N \mathcal{D}_n$ . The empirical loss  $\mathcal{L}_n(\mathbf{W}^n)$  of the  $n$ -th client can be formulated as:

$$\mathcal{L}_n(\mathbf{W}^n) = \mathbb{E}_{(x \in \mathcal{X}_n, y \in \mathcal{Y}_n) \sim \mathbb{P}_n(\mathcal{X}, \mathcal{Y})} [\ell(f^n(x; \mathbf{W}^n), y)], \quad (2)$$

where  $\ell(\cdot, \cdot)$  denotes the loss function on the clients. Following the local updates, the server  $\mathcal{S}$  performs aggregation of multiple local models’ parameters to derive the global model as  $\mathbf{W}^G \leftarrow \sum_{n=1}^N z_n \mathbf{W}^n$ .

### B. Federated UAD

As shown in Fig. 1, each client in UDA could be an industrial manufacturing enterprise, an organizational entity or a healthcare institution, etc. that faces the challenges of large raw abnormal data. Consequently, the training dataset available at the  $n$ -th client is denoted as:

$$\mathcal{D}_n^{train} = (\mathcal{X}_n, \mathcal{Y}_n) \sim \mathbb{P}_n(\mathcal{X}), \forall y \in \mathcal{Y}_n, y = 0, \quad (3)$$

and the test dataset is denoted as

$$\mathcal{D}_n^{test} = \bigcup_{n=1}^N \mathcal{D}_n^{test}, \text{ where} \quad (4)$$

$$\mathcal{D}_n^{test} = (\mathcal{X}_n, \mathcal{Y}_n) \sim \mathbb{P}_n(\mathcal{X}, \mathcal{Y}), \exists y \in \mathcal{Y}_n, y = 1,$$

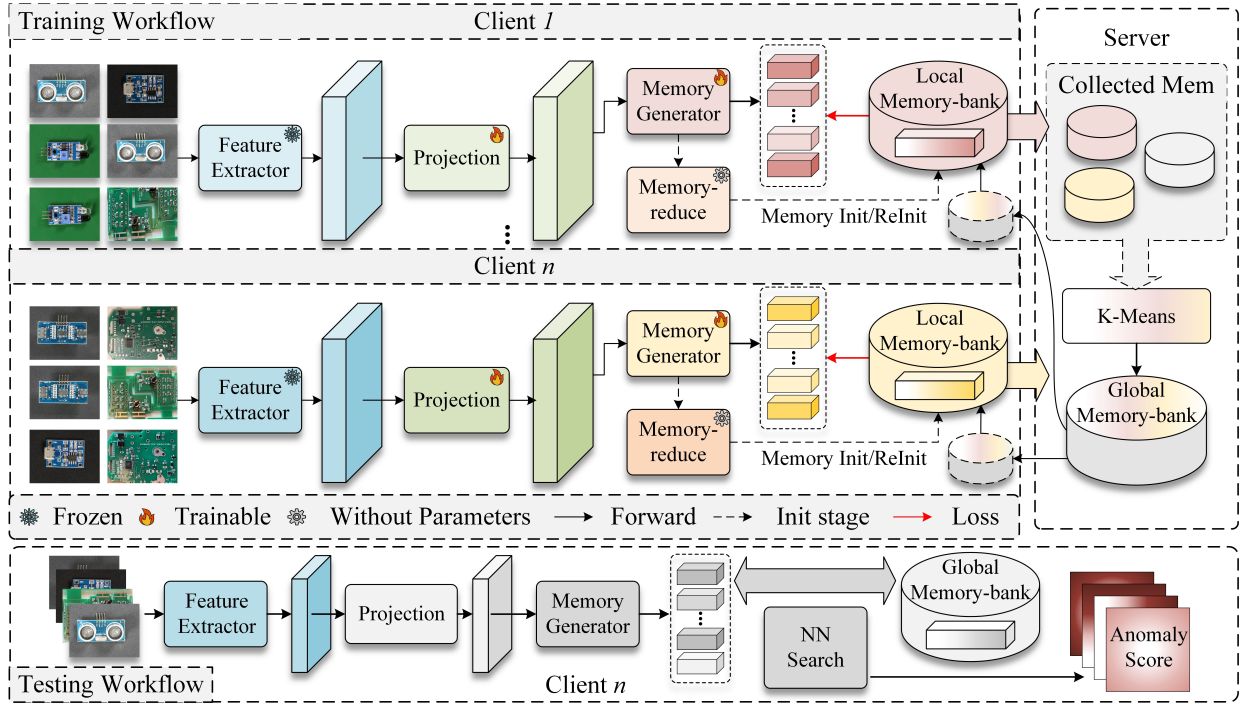


Fig. 2. Overview of our proposed FedDyMem framework. During the training phase, a pre-trained feature extractor is employed to extract features from the local training dataset, which are subsequently projected to the target domain using a projection layer. The projected features are processed through a memory generator to construct the local memory bank. In the initialization, the memory bank is further refined and reduced in size by the memory-reduce method. The server collects the local memory banks from multiple clients and aggregates them into a unified global memory bank. During the inference phase, the client utilizes the unified global memory bank to generate anomaly score maps for the test images.

where a label  $y = 0$  indicates a normal sample, while  $y = 1$  denotes an anomalous sample. In practical scenarios, as shown in Fig. 1, the distribution of client samples for the same product is different in training dataset:

$$\exists x_m \in \mathcal{D}_m^{train}, x_n \in \mathcal{D}_n^{train} \mathbb{P}_m(x_m) \neq \mathbb{P}_n(x_n), \text{ while } m \neq n. \quad (5)$$

We refer to this variation as the intra-class distribution bias. Consistent with typical federated learning, our global optimization objective remains as defined in 1. However, due to the absence of anomalous samples in the  $\mathcal{D}^{train}$ , the local model  $f^n(\cdot; \mathbf{W}^n)$  cannot effectively model  $\mathcal{X}_n \rightarrow \mathcal{Y}_n$ . Thus, the empirical loss of the  $n$ -th client in UAD is formulated as:

$$\mathcal{L}_n(\mathbf{W}^n) = \mathbb{E}_{(x \in \mathcal{X}_n) \sim \mathbb{P}_n(\mathcal{X})} [\ell(f^n(x; \mathbf{W}^n))], \quad (6)$$

where  $\ell(\cdot)$  denotes the local loss function for individual clients. It requires the  $n$ -th local model  $f^n(\cdot; \mathbf{W}^n)$  to approximate the normal sample distribution, i.e.,  $\mathbb{P}_n(\mathcal{X}^{train})$ , under the condition of intra-class bias (refer to 5). For the federated UAD, shown in Fig. 1, the global model's objective in one-class classification task is to generalize across all clients by constructing  $\mathbb{P}(\{\mathcal{X}_n^{train}\}_{n=1}^N)$ . During the testing phase, the result of a sample  $x^{test} \in \mathcal{D}^{test}$  can be expressed as follows:

$$\mathbb{1}(x^{test}) = \begin{cases} 0, & \text{if } f(x^{test}; \mathbf{W}^G) \sim \mathbb{P}(\{\mathcal{X}_n^{train}\}_{n=1}^N) \\ 1, & \text{otherwise.} \end{cases} \quad (7)$$

## IV. METHODOLOGY

### A. Overview

In this article, we propose an efficient federated learning with dynamic memory and memory-reduce for UAD, called FedDyMem. FedDyMem aims to train model parameters on datasets with locally inconsistent feature distributions and generate a global memory bank that produces uniform distributions, thereby achieving high performance on global  $\mathcal{D}^{test}$ .

On the  $n$ -th client, as shown in Fig. 2, the feature extractor, projection layer, and memory generator collaboratively generate high-quality memory representations  $\{\mathcal{M}^{n,i,t}\}_{i=0}^{|\mathcal{D}_n^{train}|}$  in the training workflow, where  $i$  denotes the  $i$ -th sample in  $\mathcal{D}_n^{train}$  and  $t$  denotes the  $t$ -th rounds. During the initialization phase ( $t = 0$ ), all memory features  $\{\mathcal{M}^{n,i,0}\}_{i=0}^{|\mathcal{D}_n^{train}|}$  extracted from training samples are processed through memory-reduce before being sent directly to the server. The local memory bank  $\mathcal{M}^{n,0}$  synchronizes with the aggregated memory bank  $\bar{\mathcal{M}}^0 \xleftarrow{agg} \{\mathcal{M}_{reduce}^{n,0}\}_{n=0}^N$  received from the server. After initialization, the extracted memory feature for sample  $i$ , denoted as  $\mathcal{M}^{n,i,t}$ , is utilized in subsequent rounds to compute the local loss  $\ell$ . This computation is performed in conjunction with the local memory bank  $\mathcal{M}^{n,t-1}$ , which is obtained from the server aggregation during the previous round. Following local training, the final updated memory features  $\mathcal{M}^{n,i,t}$  are reduced by the memory-reduce and sent to the server, summarized as  $\{\mathcal{M}^{n,i,t}\}_{i=0}^{|\mathcal{D}_n^{train}|} \rightarrow \mathcal{M}_{reduce}^{n,t}$ . On the server, representation sharing [15], [34], [53] provides distinct advan-



**Algorithm 1** Memory Generator for the sample  $x_i^n$  on Client  $n$  at Round  $t$ .

**Input:**  $n, t, x_i^n \in \mathcal{D}_n^{train}, \mathcal{F}(\cdot), \mathcal{P}^n(\cdot, \mathbf{W}^P), \mathcal{G}^n(\cdot, \mathbf{W}^G; \mathbf{G})$ .

**Output:**  $\mathcal{M}^i$ .

- 1:  $\{\mathcal{F}^{(i,l)}\}_{l=1}^L \leftarrow \mathcal{F}(x_i^n)$ , where  $L$  is determined by  $\mathcal{F}$ ;
- 2:  $\tilde{\mathcal{F}}^i \leftarrow$  Compute by Equation (8);
- 3:  $\mathcal{P}^i \leftarrow$  Compute by Equation (9);
- 4:  $\mathcal{M}^i \leftarrow \mathcal{G}^n(\mathcal{P}^i, \mathbf{W}^G; \mathbf{G})$  with Equation (10) (11);
- 5: **return**  $\mathcal{M}^i$

tages over parameter aggregation in addressing heterogeneity in unsupervised federated learning, as parameter aggregation methods suffer from privacy and intellectual property (IP) concerns [55]–[57] and introduce high communication overhead. Therefore, FedDyMem employs a memory bank sharing to ensure data privacy. In the  $t$ -th round, the server receives  $N$  local memory banks, denoted as  $\{\mathcal{M}_{reduce}^{n,t}\}_{n=0}^N$ . As shown in Fig. 2, FedDyMem employs  $K$ -means clustering algorithm, where  $K$  corresponds to the capacity of the local memory, to aggregate the diverse local memory banks into a unified global memory bank, represented as  $\bar{\mathcal{M}}^t \xrightarrow{agg} \{\mathcal{M}_{reduce}^{n,t}\}_{n=0}^N$ . The global memory bank  $\bar{\mathcal{M}}^t$  is subsequently distributed to all clients to update their respective local memory banks. Consequently, at any round  $t$ , for all  $n \in N$ , the local memory banks are synchronized such that  $\mathcal{M}^{n,t} = \bar{\mathcal{M}}^t$ . During the testing phase, the extracted memory features  $\mathcal{M}^i$  are compared against the memory bank  $\bar{\mathcal{M}}$  using the nearest neighbor search, and the anomaly score  $\mathcal{A}^i$  is computed based on the resulting metric, following the anomaly score function in [51], [58].

### B. Methodology for Obtaining $\mathcal{M}^{n,i,t}$

Locally, FedDyMem employs a frozen CNN model  $\mathcal{F}(\cdot)$  pre-trained on ImageNet to extract multi-level hierarchical features. Motivated by [51], FedDyMem performs multi-level feature fusion on the extracted features. As shown in Fig. 3, for a given sample  $x_i^n \in \mathbb{R}^{H \times W \times 3}$  which is from the  $n$ -th client's  $\mathcal{D}_n$ , the extracted features are hierarchically organized into  $L$  layers (e.g.,  $L = 5$  in the case of ResNet [59]). We define  $\mathcal{F}^{i,l} \in \mathbb{R}^{H_l \times W_l \times C_l}$  as the output features of the  $l$ -th layer, obtained from  $\mathcal{F}(x_i^n)$ , where  $i$  denotes the  $i$ -th sample from local dataset,  $l \in L$  denotes the  $l$ -th layer and  $H_l, W_l, C_l$  are the size and channel of the feature map. In multi-level feature fusion, we employ a straightforward approach combining up-sampling and feature concatenation to extract features from pre-trained CNNs. This process can be expressed as follows:

$$\tilde{\mathcal{F}}^i = f_{concat}(\{f_{up}(\mathcal{F}^{i,l}, (H_0, W_0))\}_{l=0}^L), \quad (8)$$

where  $f_{concat}(\cdot)$  represents the concatenation operation,  $f_{up}(\cdot, (H, W))$  denotes bilinear interpolation to the spatial dimensions  $(H, W)$ . Feature extractors pretrained on large-scale natural image datasets often exhibit significant distribution shifts when applied to industrial or medical images. To address this issue, we introduce a projection layer  $\mathcal{P}(\cdot, \mathbf{W}^P)$  designed to adapt the extracted features to the anomaly detection domain. As shown in Fig. 3, the projection layer is implemented

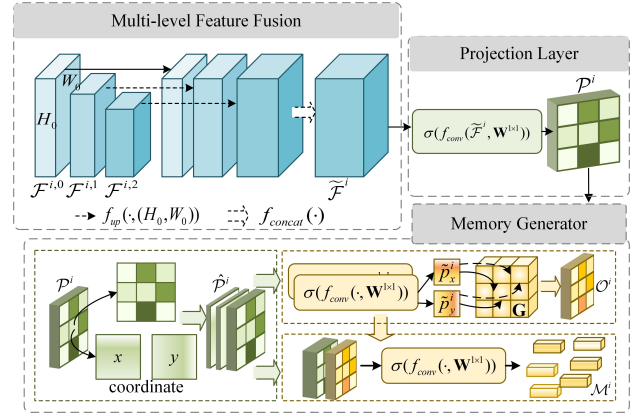


Fig. 3. The feature extraction stage in FedDyMem. Multi-level features are extracted using a pretrained CNN combined with multi-level feature fusion. These features are then projected into the anomaly detection domain through a projection layer. Subsequently, memory features are generated using a memory generator.

as a  $1 \times 1$  convolutional layer, enabling the output  $\mathcal{P}^i$  of the projection to be computed as follows:

$$\mathcal{P}^i = \sigma(f_{conv}(\tilde{\mathcal{F}}^i, \mathbf{W}^{1 \times 1})), \quad (9)$$

where  $f_{conv}(\cdot, \mathbf{W}^{q \times q})$  denotes  $q \times q$  convolution layer,  $\sigma(\cdot)$  denotes the activation function.

The memory bank-based approach [49]–[51] has demonstrated significant performance in UAD. However, the memory banks utilized in these existing methods are non-trainable, meaning they remain unchanged following initialization. Due to the local bias in feature distributions for federated UAD, using the static memory bank will lead to overfitting on domain-specific data, increasing the risk of error. Furthermore, existing methods operate mainly on a discrete feature space, which increases the variations in feature distributions between clients for normal samples [60]. In this article, we propose a memory generator that integrates spatial information and ensures the continuity of feature space. As shown in Fig. 3, the memory generator  $\mathcal{G}(\cdot, \mathbf{W}^G; \mathbf{G})$  utilizes a coordinate convolution layer  $f_{coordconv}(\cdot, \mathbf{W}^{1 \times 1})$  to encode spatial location information by incorporating additional coordinate channels, thereby facilitating the network's ability to learn spatial transformations more effectively [61]. For the projected feature  $\mathcal{P}^i$ , the result of the coordinate convolution  $\hat{\mathcal{P}}^i \in \mathbb{R}^{H \times W \times C}$  is computed as  $\hat{\mathcal{P}}^i = f_{coordconv}(f_{concat}(\{\mathcal{P}^i, \mathbf{X}, \mathbf{Y}\}, \mathbf{W}^{1 \times 1}))$ , where  $\mathbf{X}$  and  $\mathbf{Y}$  represent the Cartesian coordinates of the feature map. Then, to enhance the continuity of the memory bank, the memory generator utilizes a grid-based approach to construct a continuous feature space. We define a trainable grid space as  $\mathbf{G} \in \mathbb{R}^{H^G \times W^G \times C}$ , where  $H^G$  and  $W^G$  are hyper-parameters indicating the size of the continuous space. The memory generator maps  $\hat{\mathcal{P}}^i$  to pixel-wise coordinates  $\hat{\mathcal{P}}^i \in \mathbb{R}^{H \times W \times 2}$  through a mapping function  $\phi(\cdot, \mathbf{W}): \mathbb{R}^{H \times W \times C} \rightarrow \mathbb{R}^{H \times W \times 2}$ , implemented through two  $1 \times 1$  convolutional layers in our memory generator. A sample function  $s(\cdot, \cdot)$  is employed to extract features from the continuous space  $\mathbf{G}$  at specific coordinate values  $(p_x^i, p_y^i) \in \hat{\mathcal{P}}^i$ . The normalized

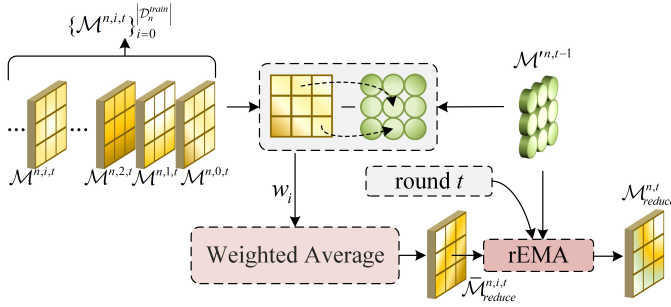


Fig. 4. Illustration of Memory-reduce.

coordinates are computed as follows:

$$\tilde{p}_x^i = \frac{(p_x^i + 1)}{2} \cdot (W^{\mathbf{G}} - 1), \quad \tilde{p}_y^i = \frac{(p_y^i + 1)}{2} \cdot (H^{\mathbf{G}} - 1), \quad (10)$$

and the result of  $s(\mathbf{G}, \tilde{\mathcal{P}}^i)$  is defined as  $\mathcal{O}^i$ . Each pixel value in  $\mathcal{O}^i$  can be sampled as:

$$\mathcal{O}_{xy}^i = \sum_{m=0}^1 \sum_{n=0}^1 w_{mn} \mathbf{G}_{\lfloor \tilde{p}_y^i \rfloor + m, \lfloor \tilde{p}_x^i \rfloor + n}, \quad \text{where} \quad (11)$$

$$w_{mn} = (1 - \lfloor \tilde{p}_x^i - (\lfloor \tilde{p}_x^i \rfloor + n) \rfloor)(1 - \lfloor \tilde{p}_y^i - (\lfloor \tilde{p}_y^i \rfloor + m) \rfloor),$$

where  $\lfloor \cdot \rfloor$  represents the floor operation. Finally, the features  $\mathcal{O}^i$ , sampled from the continuous feature space, are concatenated with the coordinate convolution outputs  $\hat{\mathcal{P}}^i$ . This concatenated tensor is then passed through a convolutional layer to generate the memory feature  $\mathcal{M}^i \in \mathbb{R}^{H \times W \times C}$  for client  $n$  at round  $t$ . The complete procedure for obtaining the memory feature is presented in Algorithm 1.

### C. Computation of Local Metric Loss: $\ell(\mathcal{M}^{n,i,t}, \mathcal{M}^{n,t-1})$

Considering the bias in feature distributions across clients, the training objective is to optimize the local memory generator to produce normal features that are more closely aligned with the shared global memory bank. FedDyMem introduces a simple metric loss to optimize the parameters of both the memory generator and the projection layer, thereby facilitating client models in generating consistent and high-quality memory features. Specifically, the local memory bank for round  $t$  is denoted as  $\mathcal{M}'^{n,t-1} = \{m'_d\}_{d=0}^D \in \mathbb{R}^{D \times C}$ , where its size is reduced to  $D$  after the initialization on the  $n$ -th client and global aggregation by the server (details of memory-reduce and aggregation are provided in Section IV-D and Section IV-E). Similar to the patch-based memory bank, the memory features  $\mathcal{M}^{n,i,t}$  can be expressed as a collection of patch features,  $\{m_{(h,w)}\}_{h=0,w=0}^{H,W}$ . The loss function  $\ell$  is defined as follow:

$$\begin{aligned} \ell(\mathcal{M}^{n,i,t}, \mathcal{M}^{n,t-1}) \\ = \frac{1}{HWK} \sum_{h,w} \sum_k \max(0, \text{dis}(m_{(h,w)}, m'_k) - th), \end{aligned} \quad (12)$$

where the function  $\text{dis}(\cdot, \cdot)$  represents the Euclidean distance metric in this article,  $th$  is a hyperparameter to mitigate overfitting. Specifically, we employ a  $K$ -nearest neighbor (KNN)

### Algorithm 2 Memory Reduce for the $\{\mathcal{M}^{n,i,t}\}_{i=0}^{|\mathcal{D}_n^{train}|}$ on Client $n$ at Round $t$ .

**Input:**  $n, t, \{\mathcal{M}^{n,i,t}\}_{i=0}^{|\mathcal{D}_n^{train}|}, \mathcal{M}^{n,t-1}$ .

**Output:**  $\mathcal{M}_{reduce}^{n,0}$ .

- 1: **for**  $i = 0$  to  $|\mathcal{D}_n^{train}|$  **do**
- 2:   **if**  $t > 0$  **then**
- 3:      $w_{i,t} \leftarrow$  Compute by Equation (15) with  $\mathcal{M}^{n,i,t}$  and  $\mathcal{M}^{n,t-1}$ ;
- 4:   **else**
- 5:      $w_{i,t} \leftarrow 1$ ;
- 6:   **end if**
- 7: **end for**
- 8:  $\bar{\mathcal{M}}_{reduce}^{n,i,t} \leftarrow$  Compute by Equation (14) with  $\{w_{i,t}\}_{i=0}^N$  and  $\{\mathcal{M}^{n,i,t}\}_{i=0}^N$ ;
- 9: **if**  $t > 0$  **then**
- 10:    $\alpha \leftarrow 1/(t+1)$ ;
- 11:    $\mathcal{M}_{reduce}^{n,t} \leftarrow$  Compute by Equation (16) with  $\bar{\mathcal{M}}_{reduce}^{n,i,t}, \mathcal{M}^{n,t-1}$  and  $\alpha$ ;
- 12: **else**
- 13:    $\mathcal{M}_{reduce}^{n,t} \leftarrow \bar{\mathcal{M}}_{reduce}^{n,i,t}$ ;
- 14: **end if**
- 15: **return**  $\mathcal{M}_{reduce}^{n,t}$

search to retrieve the top  $K$  closest features from the memory bank corresponding to the generated features. Therefore,  $k$  denotes the index in top  $K$ . FedDyMem uses the metric loss function to align the local features with the global memory bank. Following local training, the local memory bank is updated once before being uploaded to the server. This ensures that the local memory bank closely approximates the global memory bank in feature space.

### D. Memory-reduce for $\{\mathcal{M}^{n,i,t}\}_{i=0}^{|\mathcal{D}_n^{train}|} \rightarrow \mathcal{M}_{reduce}^{n,t}$

The earlier memory-based methods [49], [51] involved storing all sample memory features from the training dataset  $\mathcal{D}_n^{train}$  within the memory bank. Accordingly, the capacity of the memory bank scales proportionally with the size of the local dataset. For federated UAD, the large-scale dataset significantly challenges communication efficiency. Moreover, the varying sizes of memory banks also introduce challenges in the aggregation process. Motivated by this, FedDyMem incorporates a memory-reduce method to compress the collected memory features from the local dataset. The objective of memory-reduce can be expressed as follows:

$$\begin{aligned} \{\mathcal{M}^{n,i,t}\}_{i=0}^{|\mathcal{D}_n^{train}|} \in \mathbb{R}^{|\mathcal{D}_n^{train}| \times H \times W \times C} \\ \rightarrow \mathcal{M}_{reduce}^{n,t} \in \mathbb{R}^{H \times W \times C}, \end{aligned} \quad (13)$$

where  $\mathcal{M}^{n,i,t}$  represents the memory feature extracted by client  $n$  for the  $i$ -th sample in the training dataset  $\mathcal{D}_n^{train}$ ,  $H$  and  $W$  denote the spatial dimensions of the memory feature, and  $C$  indicates the number of feature channels.

To address the memory bank size issue, [58] employs an Exponential Moving Average (EMA) method. However, the reduced memory bank remains sensitive to the sequence

---

**Algorithm 3** Aggregation on Server  $\mathcal{S}$  for Round  $t$ .

---

**Input:**  $t, \{\mathcal{M}_{reduce}^{n,t}\}_{n=0}^N$   
**Output:**  $\bar{\mathcal{M}}^t$ .

- 1:  $m \leftarrow []$ ;
- 2:  $H, W, C \leftarrow \mathcal{M}_{reduce}^{n,t}.size()$ ;
- 3:  $K \leftarrow HW$ ;
- 4: **for**  $n = 0$  to  $N$  **do**
- 5:  $\{m_{(h,w)}^n\}_{(h=0,w=0)}^{(H,W)} \leftarrow f_{resize}(\mathcal{M}_{reduce}^{n,t}, (HW, C))$ ;
- 6:  $m \leftarrow m \cup \{m_{(h,w)}^n\}_{(h=0,w=0)}^{(H,W)}$ ;
- 7: **end for**
- 8:  $\{c_k \in \mathbb{R}^C\}_{k=0}^K \leftarrow K\text{-means}(m)$ ;
- 9:  $\bar{\mathcal{M}}^t \leftarrow f_{resize}(\{c_k\}_{k=0}^K, (H, W, C))$ ;
- 10: **return**  $\bar{\mathcal{M}}^t$

---

in which input samples are processed. In this article, we introduce a dynamic weighted average, called memory-reduce, that optimizes memory size while preserving sample order independence and effectively correlating with the number of communication rounds. As shown in Fig. 4, we aggregate all memory features, denoted as  $\{\mathcal{M}^{n,i,t}\}_{i=0}^{|\mathcal{D}_n^{train}|}$  and apply a dynamic weighted averaging operation to compute the  $\bar{\mathcal{M}}_{reduce}^{n,i,t}$  as:

$$\bar{\mathcal{M}}_{reduce}^{n,i,t} = \sum_{i=0}^{|\mathcal{D}_n^{train}|} w_{i,t} \mathcal{M}^{n,i,t} / \sum_{i=0}^{|\mathcal{D}_n^{train}|} w_{i,t}, \quad (14)$$

where the dynamic weight  $w_{i,t}$  is computed as:

$$w_{i,t} = \begin{cases} 1, & \text{if } t = 0 \\ \frac{1}{\|\mathcal{M}^{n,i,t} - \mathcal{M}^{m,t-1}\|_2}, & \text{otherwise.} \end{cases} \quad (15)$$

Here, the dynamic weight  $w_{i,t}$  is influenced by the distance between the reduced memory representation  $\mathcal{M}^{n,i,t}$  and the previous memory bank  $\mathcal{M}^{m,t-1}$ .

After computing  $\bar{\mathcal{M}}_{reduce}^{n,i,t}$ , a round-based EMA (rEMA) method is employed to update the memory bank. This approach ensures smoother and more stable updates during the training process. The update rule is defined as:

$$\mathcal{M}_{reduce}^{n,t} = \alpha \bar{\mathcal{M}}_{reduce}^{n,i,t} + (1 - \alpha) \mathcal{M}^{m,t-1} \quad (16)$$

where  $\alpha$  represents the exponential decay rate, dynamically calculated as  $\alpha = 1/(t + 1)$ . The Memory-reduce is detailed in Algorithm 2.

*E.  $\bar{\mathcal{M}}^t \xleftarrow{agg} \{\mathcal{M}_{reduce}^{n,t}\}_{n=0}^N$  on Server*

At round  $t$ , the server  $\mathcal{S}$  collects the newly generated memory banks from  $N$  clients, denoted as  $\{\mathcal{M}_{reduce}^{n,t}\}_{n=0}^N \in \mathbb{R}^{N \times H \times W \times C}$ . The objective of the server is to aggregate these memory banks into a unified, representative memory bank  $\bar{\mathcal{M}}^t$ . This process is formalized as  $\mathcal{S}(\cdot, \cdot): \mathbb{R}^{N \times H \times W \times C} \rightarrow \mathbb{R}^{H \times W \times C}$ . Representation-based federated learning approaches, such as those proposed in [34], [63], utilize weighted aggregation of class prototypes during model updates. However, significant feature bias in the early training stages leads to aggregated memory that deviates significantly from the client-specific memory, which often contains incomplete product types. This misalignment hinders

---

**Algorithm 4** Initialization at Round 0.

---

**Input:**  $\{\mathcal{D}_n^{train}\}_{n=0}^N, \mathcal{F}(\cdot), \mathcal{P}^n(\cdot, \mathbf{W}^P), \mathcal{G}^n(\cdot, \mathbf{W}^G; \mathbf{G})$ .  
**Output:**  $\{\mathcal{M}_{reduce}^{n,0}\}_{n=0}^N$

- 1: **for** each client  $n$  **in parallel do**
- 2: Initialize  $\mathbf{W}^P, \mathbf{W}^G$  randomly for  $\mathcal{P}^n(\cdot, \mathbf{W}^P), \mathcal{G}^n(\cdot, \mathbf{W}^G; \mathbf{G})$ ;
- 3: Initialize  $\mathbf{G}$  by Xavier normal initialization method [62] for  $\mathcal{G}^n(\cdot, \mathbf{W}^G; \mathbf{G})$ ;
- 4: **for**  $i = 0$  to  $|\mathcal{D}_n^{train}|$  **do**
- 5:  $\mathcal{M}^i \leftarrow$  Compute by Algorithm 1 with  $t = 0, n, x_i^n, \mathcal{F}(\cdot), \mathbf{W}^P, \mathbf{W}^G, \mathbf{G}$ ;
- 6: **end for**
- 7:  $\{\mathcal{M}^{n,i,0}\}_{i=0}^{|\mathcal{D}_n^{train}|} \leftarrow [\mathcal{M}^0, \mathcal{M}^1, \dots]$ ;
- 8:  $\mathcal{M}_{reduce}^{n,0} \leftarrow$  Compute by Algorithm 2 with  $n, t = 0$  and  $\{\mathcal{M}^{n,i,0}\}_{i=0}^{|\mathcal{D}_n^{train}|}$ ;
- 9:  $\mathbf{W}^{P,n,0} \leftarrow \mathbf{W}^P, \mathbf{W}^{G,n,0} \leftarrow \mathbf{W}^G, \mathbf{G}^{n,0} \leftarrow \mathbf{G}$
- 10: **end for**
- 11:  $\{\mathcal{M}_{reduce}^{n,0}\}_{n=0}^N \leftarrow [\mathcal{M}_{reduce}^{0,0}, \mathcal{M}_{reduce}^{1,0}, \dots]$ ;
- 12:  $\bar{\mathcal{M}}^0 \leftarrow$  Compute by Algorithm 3 with  $t = 0$  and  $\{\mathcal{M}_{reduce}^{n,0}\}_{n=0}^N$ ;
- 13: **for**  $n = 0$  to  $N$  **do**
- 14:  $\mathcal{M}^{n,0} \leftarrow \bar{\mathcal{M}}^0$ ;
- 15: **end for**
- 16: **return**  $\{\mathcal{M}^{n,0}\}_{n=0}^N \leftarrow [\mathcal{M}^{0,0}, \mathcal{M}^{1,0}, \dots]$

---

convergence, posing a challenge for clients with limited data diversity. Thus, we employ a clustering-based approach to aggregate the collected memory banks effectively. Specifically, the memory features are represented as  $N \times H \times W$  patch features, denoted by  $m_{(h,w)}^n \in \mathbb{R}^C$ . These patch features are subsequently clustered using the  $K$ -means algorithm, where the number of clusters,  $K$ , corresponds to  $H \times W$ . The clustering results indicate the overall distribution and similarity relationships between the patch-level features stored across all banks at the current stage of the process. Cluster centers describe the representative features of a memory bank. Let  $c_k \in \mathbb{R}^C$  denote the center of the  $k$ -th cluster, serving as a global memory bank updated by  $\bar{\mathcal{M}}^t = f_{resize}(\{c_k\}_{k=0}^K, (H, W, C))$  and shared across individual clients,  $\forall n \in N, \mathcal{M}^{n,t} = \bar{\mathcal{M}}^t$ . The aggregation methodology is outlined in Algorithm 3, while the comprehensive training procedure for FedDyMem is presented in Algorithm 5.

*F. Privacy Preserving Discussion*

FedDyMem facilitates the exchange of statistical information, i.e., memory banks, between the clients and the server, instead of transmitting model parameters, thereby enhancing privacy protection [34]. The memory features that are transmitted are derived from multi-layer low-dimension representations, which is an irreversible process [65]. In practice, additional privacy-preserving techniques can be incorporated into the FedDyMem framework to further improve system reliability [66] and ensure robust data protection [67].

**Algorithm 5** Training for FedDyMem.

---

**Input:**  $N$  Clients  $\{\mathcal{C}_n\}_{n=1}^N$  with  $\{\mathcal{D}_n^{train}\}_{n=0}^N$ , one server  $\mathcal{S}$ , the number of rounds  $T$ , the local epochs  $E$ .

- 1:  $\{\mathcal{M}^{n,0}\}_{n=0}^N \leftarrow$  Initialization by Algorithm 4;
- 2: **for**  $t = 1$  to  $T$  **do**
- 3:   **for** each client  $n$  **in parallel do**
- 4:      $\mathcal{M}_{reduce}^{n,t} \leftarrow$  ClientUpdate( $n, t, E, \mathcal{D}_n^{train}$ );
- 5:   **end for**
- 6:    $\{\mathcal{M}_{reduce}^{n,t}\}_{n=0}^N \leftarrow$  Collection all memory bank from  $N$  clients;
- 7:    $\bar{\mathcal{M}}^t \leftarrow$  Upload  $\{\mathcal{M}_{reduce}^{n,t}\}_{n=0}^N$  to  $\mathcal{S}$  and computed by Algorithm 3;
- 8: **end for**
- 9: Save all well trained  $\{\mathbf{W}^{\mathcal{P},n,T}, \mathbf{W}^{\mathcal{G},n,T}, \mathbf{G}^{n,T}\}_{n=0}^N$  and  $\bar{\mathcal{M}}^T$  locally.

*ClientUpdate*( $n, t, E, \mathcal{D}_n^{train}$ ):

- 10: **for**  $e = 0$  to  $E$  **do**
- 11:   **for**  $i = 0$  to  $|\mathcal{D}_n^{train}|$  **do**
- 12:      $\mathcal{M}^i \leftarrow$  Compute by Algorithm 1 with  $t, n, x_i^n$ ;
- 13:      $\ell \leftarrow$  Compute loss by Equation (12) with  $\mathcal{M}^i$  and  $\mathcal{M}^{n,t-1}$ ;
- 14:     Update  $\{\mathbf{W}^{\mathcal{P},n,t}, \mathbf{W}^{\mathcal{G},n,t}, \mathbf{G}^{n,t}\}$  by  $\ell$  and Adam Optimizer [64];
- 15:   **end for**
- 16: **end for**
- 17:  $\{\mathcal{M}^{n,i,t}\}_{i=0}^{|\mathcal{D}_n^{train}|} \leftarrow [\mathcal{M}^0, \mathcal{M}^1, \dots]$ ;
- 18:  $\mathcal{M}_{reduce}^{n,t} \leftarrow$  Compute by Algorithm 2 with  $n, t$  and  $\{\mathcal{M}^{n,i,t}\}_{i=0}^{|\mathcal{D}_n^{train}|}$ ;
- 19: **return**  $\mathcal{M}_{reduce}^{n,t}$

---

## V. CONVERGENCE ANALYSIS

We provide the convergence analysis for FedDyMem considering the non-convex nature of its loss function. Some common assumptions based on existing frameworks are reasonably presented below:

**Assumption 1 (Piecewise  $L_2$ -Lipschitz Smooth).** Let  $\text{dis}(m_{(h,w)}, m'_k) = th$  denote the discontinuity point. For any  $t, t' > 0$ , there exists  $L > 0$  satisfying:

$$\begin{aligned} \|\nabla\ell(\mathcal{M}^{n,i,t}, \mathcal{M}^{n,t-1}) - \nabla\ell(\mathcal{M}^{n,i,t'}, \mathcal{M}^{n,t'-1})\|_2 \\ \leq L\|\mathcal{M}^{n,i,t} - \mathcal{M}^{n,i,t'}\|_2. \end{aligned} \quad (17)$$

**Assumption 2 (Bounded Gradients).** The gradients of the loss function are bounded, i.e., there exists  $G > 0$  satisfying:

$$\|\nabla\ell(\mathcal{M}^{n,i,t}, \mathcal{M}^{n,t-1})\|_2 \leq G. \quad (18)$$

**Assumption 3 (Unbiased Gradient and Bounded Variance).** The stochastic gradient  $g_t$  is an unbiased estimate of the true gradient, i.e.,  $\mathbb{E}[g_t] = \nabla\ell(\mathcal{M}^{n,i,t}, \mathcal{M}^{n,t-1})$ . Furthermore, the variance of  $g_t$  is bounded, i.e., there exists  $\sigma^2 > 0$  satisfying:

$$\mathbb{E}[\|g_t - \nabla\ell(\mathcal{M}^{n,i,t}, \mathcal{M}^{n,t-1})\|_2^2] \leq \sigma^2. \quad (19)$$

**Assumption 4.** Based on the loss function's structure, the hyperparameter  $th$  is constrained as:

$$th \in \left[ \min_{h,w,k} \text{dis}(m_{(h,w)}, m'_k), \frac{1}{HWK} \sum_{h,w,k}^{H,W,K} \text{dis}(m_{(h,w)}, m'_k) \right]$$

, ensuring the loss function  $\ell$  remains finite and satisfies the operational properties in Assumptions 1-4.

**Theorem 1 (Loss Reduction).** For any client, after every communication round, when the learning rate satisfies  $0 < \eta < \frac{2}{L}$ , and letting  $\mathcal{M}^t = \mathcal{M}^{n,i,t}, \mathcal{M}' = \mathcal{M}^{n,t-1}$ , the expected loss after  $T$  iterations satisfies:

$$\begin{aligned} \mathbb{E}[\ell(\mathcal{M}^T, \mathcal{M}')] &\leq \ell(\mathcal{M}^{n,i,1}, \mathcal{M}^{n,0}) + \frac{T\eta^2 L\sigma^2}{2} \\ &\quad - \left(\eta - \frac{\eta^2 L}{2}\right) \sum_{t=1}^{T-1} \mathbb{E}[\|\nabla\ell(\mathcal{M}^t, \mathcal{M}')\|_2^2]. \end{aligned} \quad (20)$$

*Proof.* For each iteration, based on the Assumptions above, the loss function satisfies:

$$\begin{aligned} \mathbb{E}[\ell(\mathcal{M}^{t+1}, \mathcal{M}')] &\leq \mathbb{E}[\ell(\mathcal{M}^t, \mathcal{M}')] - \eta\mathbb{E}[\|\nabla\ell(\mathcal{M}^t, \mathcal{M}')\|_2^2] \\ &\quad + \frac{\eta^2 L}{2} \mathbb{E}[\|\nabla\ell(\mathcal{M}^t, \mathcal{M}')\|_2^2] \\ &\leq \mathbb{E}[\ell(\mathcal{M}^t, \mathcal{M}')] + \frac{\eta^2 L\sigma^2}{2} \\ &\quad - \left(\eta - \frac{\eta^2 L}{2}\right) \mathbb{E}[\|\nabla\ell(\mathcal{M}^t, \mathcal{M}')\|_2^2]. \end{aligned}$$

After  $T$  iterations, we obtain:

$$\begin{aligned} \mathbb{E}[\ell(\mathcal{M}^T, \mathcal{M}')] &\leq \ell(\mathcal{M}^{n,i,1}, \mathcal{M}^{n,0}) + \frac{T\eta^2 L\sigma^2}{2} \\ &\quad - \left(\eta - \frac{\eta^2 L}{2}\right) \sum_{t=1}^{T-1} \mathbb{E}[\|\nabla\ell(\mathcal{M}^t, \mathcal{M}')\|_2^2]. \end{aligned}$$

Theorem 1 expresses that by appropriately selecting  $\eta$  and  $\sigma$ , the penalty term  $\frac{T\eta^2 L\sigma^2}{2}$  in the loss descent inequality can be controlled, such that the term  $-\left(\eta - \frac{\eta^2 L}{2}\right) \sum_{t=1}^{T-1} \mathbb{E}[\|\nabla\ell(\mathcal{M}^t, \mathcal{M}')\|_2^2]$  plays a dominant role in the gradient descent of the loss function. In the subsequent Theorem 2, we provide the convergence results of the model.

**Theorem 2 (FedDyMem Convergence).** Based on the previous assumptions and Theorem 1, when  $th$  satisfies the constraint in Assumption 4, for any  $\epsilon > \frac{\eta L\sigma^2}{2(\eta - \frac{\eta^2 L}{2})}$ , there exists:

$$T = \frac{\ell(\mathcal{M}^{n,i,1}, \mathcal{M}^{n,0}) - \ell}{\epsilon \left(\eta - \frac{\eta^2 L}{2}\right)},$$

such that for  $t > T$ ,

$$\frac{1}{T} \sum_{t=1}^{T-1} \mathbb{E}[\|\nabla\ell(\mathcal{M}^{n,i,t}, \mathcal{M}^{n,t-1})\|_2^2] \leq \epsilon. \quad (21)$$

*Proof.* From Theorem 1, we have:

$$\mathbb{E}[\ell(\mathcal{M}^T, \mathcal{M}')] \leq \ell(\mathcal{M}^{n,i,1}, \mathcal{M}^{m,0}) + \frac{T\eta^2 L\sigma^2}{2} - \left( \eta - \frac{\eta^2 L}{2} \right) \sum_{t=1}^{T-1} \mathbb{E}[\|\nabla \ell(\mathcal{M}^t, \mathcal{M}')\|_2^2].$$

Since  $\ell(\mathcal{M}, \mathcal{M}')$  has a non-negative lower bound  $\underline{\ell}$ , satisfying  $0 < \underline{\ell} < \ell$ , we write:

$$\begin{aligned} \underline{\ell} &\leq \ell(\mathcal{M}^T, \mathcal{M}') \\ &\leq \ell(\mathcal{M}^{n,i,1}, \mathcal{M}^{m,0}) + \frac{T\eta^2 L\sigma^2}{2} \\ &\quad - \left( \eta - \frac{\eta^2 L}{2} \right) \sum_{t=1}^{T-1} \mathbb{E}[\|\nabla \ell(\mathcal{M}^t, \mathcal{M}')\|_2^2]. \end{aligned}$$

After rearranging and simplifying:

$$\frac{1}{T} \sum_{t=1}^{T-1} \mathbb{E}[\|\nabla \ell(\mathcal{M}^t, \mathcal{M}')\|_2^2] \leq \frac{\ell(\mathcal{M}^{n,i,1}, \mathcal{M}^{m,0}) - \underline{\ell}}{T(\eta - \frac{\eta^2 L}{2})} + \frac{\eta L\sigma^2}{2(\eta - \frac{\eta^2 L}{2})}.$$

Letting this upper bound be less than or equal to  $\epsilon$ , we solve for  $T$ :

$$T \geq \frac{\ell(\mathcal{M}^{n,i,1}, \mathcal{M}^{m,0}) - \underline{\ell}}{\epsilon(\eta - \frac{\eta^2 L}{2})}.$$

## VI. EXPERIMENTS

All experiments presented in this article were implemented and conducted using the PyTorch framework. Model training was performed on a high-performance computing system equipped with AMD EPYC 9554 64-core processors and eight NVIDIA GeForce RTX A6000 GPUs, each possessing 48 GB of memory, to ensure accelerated computation.

### A. Experimental Settings

1) *Datasets:* In this article, we combined 6 image anomaly detection datasets containing different types of data, covering various industrial inspection scenarios and medical imaging domains, to evaluate the performance of FedDyMem. These datasets are as follows:

- **Mixed-Brain-AD(Brain):** We combined 3 brain image diagnostic datasets, including Brain-Tumor [2], BraTS2021<sup>1</sup> [68] and HeadCT<sup>2</sup> [69]. These datasets, consisting of both MRI and CT images, were distributed across different clients in a heterogeneous manner to represent a mixture of various image types.
- **Mixed-ChestXray-AD(X-ray):** Three diagnostic chest X-ray datasets, including ChestXRay2017 [70], RSNA<sup>3</sup> [71], and VinDr-CXR<sup>4</sup> [72], were employed in this article. These datasets were derived from distinct medical institutions, ensuring a diverse and heterogeneous data distribution, which is essential for the federated UAD.

<sup>1</sup><https://www.kaggle.com/datasets/masoudnickparvar/brain-tumor-mri-dataset>

<sup>2</sup><https://www.kaggle.com/datasets/felipekitamura/head-ct-hemorrhage>

<sup>3</sup><https://www.kaggle.com/c/rsna-pneumonia-detection-challenge>

<sup>4</sup><https://www.kaggle.com/c/vinbigdata-chest-xray-abnormalities-detection>

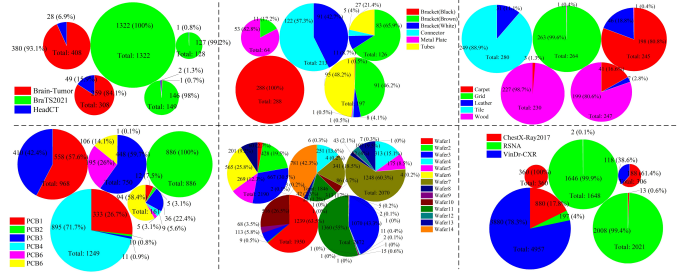


Fig. 5. Summary of the dataset distribution on five clients. The relative sizes of the pie in the chart illustrate the total data volume across individual clients. Distinct colors within each pie represent different product types.

- **Mixed-PCB-AD(PCB):** We investigate 2 datasets containing PCB anomalies, namely VisA [73] and VISION [74], and integrate them to create the Mixed-PCB dataset. The VisA dataset includes six different types of PCB products, while the VISION dataset encompasses two types. Consequently, the Mixed-PCB-AD dataset provides a total of 8 distinct types of PCB product images, facilitating simulation in federated UAD.
- **MVTec [75]:** In this article, we utilize 5 texture classes(carpet, grid, leather, tile, and wood) from the MVTEC dataset, which includes mask annotations, to simulate industrial federated anomaly detection scenarios.
- **MetalPartsAD(MPDD) [76]:** The MPDD comprises images of 6 types of metal parts, each captured under varying conditions of spatial orientation, object positioning, and camera distance. These images are further characterized by diverse lighting intensities and non-homogeneous backgrounds, providing a comprehensive dataset for our federated UAD.
- **TextureAD-Wafer(Wafer) [19]:** TextureAD-Wafer comprises a dataset of 14 distinct wafer products, each imaged using an industrial-grade, high-resolution optical camera. This dataset also explores these wafer products under various optical conditions, thus providing a rich federated UAD simulate environment with diverse feature distributions.

2) *Scenes with Feature Distribution Bias:* In this article, we aim to simulate heterogeneous feature distributions across 5 clients by all samples from the same normal categories with different product types. We employ a Dirichlet distribution to allocate data, where each product type, though labeled as normal, is distributed to various clients. We set the Dirichlet parameter  $\alpha = 0.1$  to accentuate the variances in data distribution across clients, thus simulating more realistic and challenging multi-client scenarios typically encountered in federated UAD. Fig. 5 illustrates the results of this partitioning approach across all datasets.

3) *Implementation Details:* The frozen feature extractor used in our experiments is the Wide-ResNet-50 model pre-trained on the ImageNet dataset. For FedDyMem, the hyperparameters  $H^G$  and  $W^G$  are set to 8, and  $th$  is set to 0.01. All baseline models are constructed using the Wide-ResNet-50, with all parameters comprehensively aggregated. The parameter  $K$  for the KNN algorithm is set to 3. For a





TABLE I  
COMPARISON OF IMAGE-AUROC (%) RESULTS ON SIX DATASET

Methods	Communication Parameters	Wafer	PCB	MVTec	MPDD	Brain	X-ray
Local	-	57.35(±0.71)	51.89(±0.76)	75.94(±0.39)	54.39(±0.77)	50.66(±0.87)	61.02(±0.58)
FedAvg	Model Parameters: ≈ 10.66M, (SCAFFOLD) ≈ 10.66M * 2	63.91(±0.36)	54.18(±0.33)	80.32(±0.81)	61.87(±0.76)	50.16(±0.63)	61.48(±0.56)
FedProx		63.98(±0.51)	54.11(±0.48)	80.22(±0.78)	61.83(±0.61)	50.47(±0.34)	61.45(±0.66)
FedPHP		63.94(±0.56)	54.13(±0.36)	80.19(±0.62)	61.80(±0.63)	50.38(±0.39)	61.45(±0.37)
APPLE		65.92(±0.33)	56.79(±0.65)	82.43(±0.51)	61.03(±0.77)	50.82(±0.45)	68.47(±0.51)
FedBN		63.89(±0.35)	54.09(±0.79)	80.13(±0.77)	61.90(±0.61)	50.04(±0.54)	61.45(±0.72)
SCAFFOLD		66.53(±0.85)	63.56(±0.37)	83.26(±0.37)	59.41(±0.80)	49.90(±0.52)	72.52(±0.52)
DBE		64.12(±0.49)	53.78(±0.38)	79.78(±0.90)	61.78(±0.51)	50.06(±0.85)	62.77(±0.61)
<b>Ours</b>	Memory Size: ≈ <b>5.62M</b>	<b>71.96(±0.32)</b>	<b>83.34(±0.45)</b>	<b>99.24(±0.36)</b>	<b>83.93(±0.77)</b>	<b>89.27(±0.45)</b>	<b>80.30(±0.36)</b>

TABLE II  
COMPARISON OF ABNORMAL LOCATION CAPABILITY ON FOUR DATASETS

Methods	Wafer		PCB		MVTec		MPDD	
	P-AUROC(%)	PRO(%)	P-AUROC(%)	PRO(%)	P-AUROC(%)	PRO(%)	P-AUROC(%)	PRO(%)
Local	58.27(±1.20)	47.76(±0.52)	68.12(±1.11)	45.86(±1.31)	72.63(±0.98)	56.97(±0.48)	87.02(±1.05)	51.31(±0.73)
FedAvg	66.56(±0.70)	67.00(±0.30)	69.30(±0.34)	54.04(±0.57)	76.16(±0.73)	53.35(±1.49)	91.67(±0.94)	55.07(±1.25)
FedProx	66.41(±0.74)	67.25(±0.33)	69.10(±1.28)	54.04(±1.28)	76.08(±1.28)	53.62(±0.70)	91.59(±1.02)	54.96(±1.16)
FedPHP	66.44(±1.38)	67.16(±0.38)	69.11(±0.42)	54.23(±1.16)	76.03(±0.57)	53.37(±0.47)	91.56(±0.73)	54.86(±1.42)
APPLE	69.88(±0.95)	69.02(±0.42)	71.34(±0.85)	60.11(±1.45)	78.06(±1.08)	54.14(±1.16)	92.12(±1.19)	55.84(±0.76)
FedBN	66.32(±0.57)	67.16(±0.68)	68.91(±0.82)	54.21(±1.07)	75.92(±1.34)	53.48(±0.79)	91.59(±0.38)	54.92(±0.82)
SCAFFOLD	68.75(±1.19)	68.74(±1.03)	77.18(±0.54)	66.43(±0.58)	80.81(±0.35)	55.79(±1.30)	93.47(±0.74)	58.71(±0.84)
DBE	66.95(±1.07)	68.46(±1.05)	72.95(±1.35)	57.89(±0.75)	76.18(±0.89)	53.86(±0.58)	92.66(±1.36)	55.76(±0.95)
<b>Ours</b>	<b>78.40(±1.31)</b>	<b>74.91(±0.54)</b>	<b>96.03(±0.79)</b>	<b>81.09(±1.31)</b>	<b>97.04(±0.56)</b>	<b>86.81(±1.13)</b>	<b>98.97(±1.39)</b>	<b>79.43(±1.15)</b>

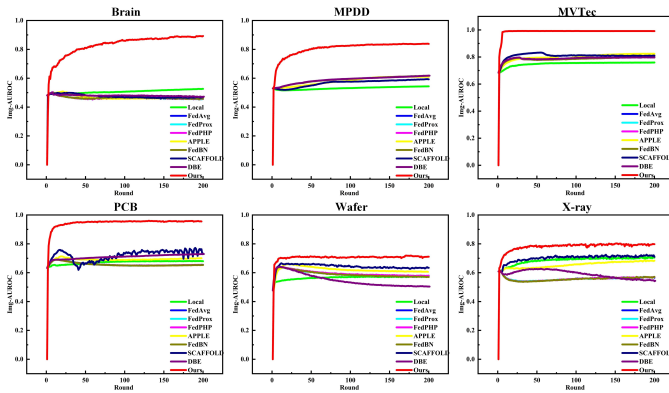


Fig. 7. Illustration of I-AUROC test accuracy comparing FedDyMem and baseline models.

### C. Performance Comparisons with Existing Methods

To demonstrate the superior performance of FedDyMem, we conducted extensive comparative analyses with 8 baseline models. These include the basic federated learning algorithm FedAvg [54], the regularization-based FedProx [22], the personalized-based FedPHP [77] and APPLE [29]. Additionally, we compared against domain-skew-oriented methods such as FedBN [23] and SCAFFOLD [20], as well as the model-splitting method DBE [35] and a purely local training scheme (Local).

1) *Training Process*: Fig. 7 illustrates the I-AUROC performance of the FedDyMem training process in comparison with baseline models on all datasets. FedDyMem achieves superior testing accuracy compared to other baseline models, while

also exhibiting a more stable training process. Specifically, the baseline models exchange parameters exclusively during communication rounds, introducing a distribution bias for memory features. This limitation prevents the models from achieving suboptimal solutions.

2) *Communication Cost*: In federated learning, communication efficiency is crucial for practical deployment, especially in bandwidth-constrained or latency-sensitive environments. As shown in Table I, most existing methods (e.g., FedAvg, FedProx, APPLE) require extensive communication of full model parameters, which amount to approximately 10.66 MB per communication round. In contrast, our approach only requires the exchange of a memory bank of approximately 5.62MB during each communication round. This substantially reduces communication overhead, enabling faster convergence in settings with limited communication resources.

3) *Anomaly Detection*: As shown in Table I, the performance of FedDyMem is evaluated across six datasets and compared with a set of baseline models. Conventional federated learning methods such as FedAvg, FedProx, and FedPHP show similar performance, typically outperforming the Local, but remaining below 65% AUROC on most datasets (e.g., 64% on Wafer). APPLE and FedBN show improvements over FedAvg-like methods (e.g., 65.92% AUROC on Wafer for APPLE), but their effectiveness decreases on more challenging datasets such as Brain, where AUROC remains below 51%. SCAFFOLD achieves relatively better results (e.g., 72.52% on X-ray), but provides limited gains on PCB, Brain, and MPDD. Similarly, DBE shows incremental improvements across all benchmarks but fails to match our method. In contrast, our proposed

TABLE III  
ABLATION STUDY OF STRUCTURE FOR FEDDYMEM.

+Projection	+Memory Generator	+K-means	I-AUROC (%)						P-AUROC (%)			
			Wafer	PCB	MVTec	MPDD	Brain	X-ray	Wafer	PCB	MVTec	MPDD
-	-	-	67.69	69.58	85.86	70.41	69.03	68.92	70.23	83.23	85.22	94.19
✓	-	-	68.93	74.10	87.27	78.28	74.95	72.71	74.29	89.26	90.84	95.77
✓	✓	-	70.96	81.26	92.76	81.05	85.94	78.12	77.01	94.97	96.10	97.96
✓	✓	✓	<b>71.96</b>	<b>83.34</b>	<b>99.24</b>	<b>83.93</b>	<b>89.27</b>	<b>80.30</b>	<b>78.40</b>	<b>96.03</b>	<b>97.04</b>	<b>98.97</b>

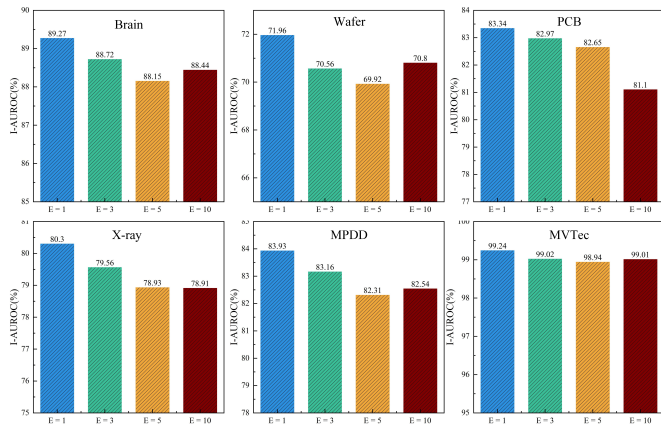


Fig. 8. Impact of different local epochs on clients.

approach consistently achieves the highest I-AUROC scores across all six anomaly detection benchmarks. Specifically, our method achieves 71.96% for Wafer, 83.34% for PCB, 99.24% for MVTEC, 83.93% for MPDD, 89.27% for Brain, and 80.30% for X-ray.

4) *Anomaly Localization*: As shown in Table II we evaluate the abnormal localization performance on four datasets (Wafer, PCB, MVTEC, and MPDD), as the Brain and X-ray do not provide region-level labels. To measure both detection capability and localization accuracy, each method is evaluated using two metrics, P-AUROC and PRO. The baseline method Local exhibits the lowest overall performance, with approximately 58.27% in P-AUROC and 47.76% in PRO on the Wafer dataset, and similar results across the other datasets. This proves that there are distribution bias in the raw dataset. For the federated learning approaches, FedAvg, FedProx, and FedPHP demonstrate closely aligned performance improvements. APPLE delivers further performance gains, achieving a P-AUROC of up to 69.88% on the Wafer dataset. In contrast, our proposed method achieves superior performance across all evaluated datasets and metrics. These consistent and robust improvements highlight the effectiveness and adaptability of our approach in tackling federated anomaly localization tasks across diverse application scenarios.

#### D. Ablation Study

1) *Impact of Local Training Epochs*: Fig. 8 illustrates the impact of varying the number of local training epochs ( $E$ ) on the performance of federated learning across all datasets. A clear trend emerges where increasing  $E$  generally results

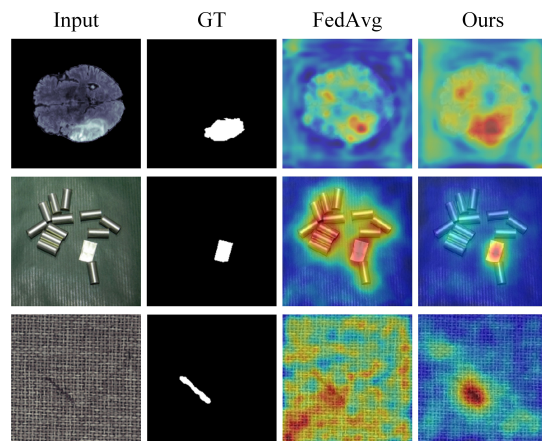


Fig. 9. Qualitative comparison of FedAvg and our proposed method. The results were obtained from a randomly selected client using a global memory bank.

in a performance decline. For example, in the Wafer dataset, accuracy drops from 71.96% at  $E = 1$  to 69.92% at  $E = 5$ . Similarly, the PCB dataset demonstrates a decrease in performance, with accuracy falling from 83.34% at  $E = 1$  to 82.65% at  $E = 5$ . MPDD, Brain, and X-ray also exhibit gradual performance degradation with higher  $E$  values. This phenomenon can be attributed to the heterogeneous data distribution across clients. As the number of local training epochs increases, the local models tend to overfit their respective client datasets, leading to a decrease in the effectiveness of the globally aggregated memory features.

2) *Effect of Projection Layer*: The ablation study is presented in Table III shows the significant impact of incorporating a projection layer on the performance of the proposed FedDyMem framework. The baseline configuration used for comparison consists of memory-reduction and memory feature average aggregation mechanisms, without additional architectural enhancements. Specifically, introducing the projection layer improves both I-AUROC and P-AUROC metrics across all datasets. For example, the I-AUROC for Wafer increases from 67.69% to 68.93%, and the P-AUROC improves from 70.23% to 74.29%. These results demonstrate that the projection layer effectively enhances feature representations.

3) *Effect of Memory Generator*: The integration of the memory generator significantly improves the anomaly detection performance of FedDyMem across different datasets. For example, the memory generator increases the I-AUROC from 68.93% to 70.96% on the wafer dataset and from 74.10% to 81.26% on the PCB dataset. A similar trend is observed for

P-AUROC, with increases from 74.29% to 77.01% on Wafer and from 89.26% to 94.97% on PCB. These improvements demonstrate the ability of the memory generator to effectively refine feature representations.

4) *Effect of K-means*: The addition of  $K$ -means to the FedDyMem framework resulted in a consistent improvement across all evaluated metrics. When combined with the projection layer and memory generator,  $K$ -means further improves I-AUROC, achieving increases such as from 70.96% to 71.96% for Wafer and from 81.26% to 83.34% for PCB. Similarly, P-AUROC improves significantly with values such as Wafer from 77.01% to 78.40% and PCB from 94.97% to 96.03%.

### E. Qualitative Results

Fig. 9 provides a qualitative comparison of the prediction results between FedAvg and the proposed FedDyMem method under an identical experimental setting. The FedDyMem approach exhibits a notable improvement in prediction quality, with substantially fewer noisy regions evident in the results. Following the methodology in [58], the anomaly score heatmaps are upsampled to match the spatial resolution of the input image and subsequently refined using Gaussian filtering with  $\sigma = 4$ , ensuring smoother and more coherent boundaries. Furthermore, min-max normalization is applied to standardize the range of anomaly scores, facilitating clearer visualization and interpretation of the results.

## VII. CONCLUSION

In this article, we propose an efficient federated learning with dynamic memory and memory-reduce, called FedDyMem to address the federated UAD problem. To tackle the challenges posed by multi-client data distribution bias in real-world industrial and medical scenarios, FedDyMem introduces a memory generator and a loss function based on distance metrics to dynamically generate high-quality memory banks. To enhance communication efficiency, a memory-reduce method is incorporated to decrease the size of the memory banks, thereby minimizing communication costs. During the aggregation phase,  $K$ -means is employed on the server to mitigate ambiguity and confusion across memory banks from different clients. Extensive experimental results demonstrate that the proposed method significantly outperforms existing baselines. Future work will focus on optimizing the model heterogeneity adaptation to further enhance the scalability and generalization of the proposed framework.

## REFERENCES

- [1] G. Xie, J. Wang, J. Liu, J. Lyu, Y. Liu, C. Wang, F. Zheng, and Y. Jin, "Im-iad: Industrial image anomaly detection benchmark in manufacturing," *IEEE Transactions on Cybernetics*, 2024.
- [2] Y. Cai, W. Zhang, H. Chen, and K.-T. Cheng, "Medianomaly: A comparative study of anomaly detection in medical images," *arXiv preprint arXiv:2404.04518*, 2024.
- [3] G. Yang, Z. Yang, S. Cui, C. Song, J. Wang, and H. Wei, "Clustering federated learning for wafer defects classification on statistical heterogeneous data," *IEEE Transactions on Instrumentation and Measurement*, 2024.
- [4] Y. Wu, C. Desrosiers, and A. Chaddad, "Facmic: Federated adaptive clip model for medical image classification," in *International Conference on Medical Image Computing and Computer-Assisted Intervention*. Springer, 2024, pp. 531–541.
- [5] X.-C. Li and D.-C. Zhan, "Fedrs: Federated learning with restricted softmax for label distribution non-iid data," in *Proceedings of the 27th ACM SIGKDD conference on knowledge discovery & data mining*, 2021, pp. 995–1005.
- [6] S. Saha, A. Hota, A. K. Chattopadhyay, A. Nag, and S. Nandi, "A multifaceted survey on privacy preservation of federated learning: progress, challenges, and opportunities," *Artificial Intelligence Review*, vol. 57, no. 7, p. 184, 2024.
- [7] Y. Zhao, Q. Liu, P. Liu, X. Liu, and K. He, "Medical federated model with mixture of personalized and shared components," *IEEE Transactions on Pattern Analysis and Machine Intelligence*, 2024.
- [8] W. Li, K. Fan, K. Yang, Y. Yang, and H. Li, "Pbfl: Privacy-preserving and byzantine-robust federated learning empowered industry 4.0," *IEEE Internet of Things Journal*, 2023.
- [9] R. Zhang, H. Li, L. Tian, M. Hao, and Y. Zhang, "Vertical federated learning across heterogeneous regions for industry 4.0," *IEEE Transactions on Industrial Informatics*, 2024.
- [10] Y. Jin, Y. Liu, K. Chen, and Q. Yang, "Federated learning without full labels: A survey," *arXiv preprint arXiv:2303.14453*, 2023.
- [11] W. Zhuang, X. Gan, Y. Wen, S. Zhang, and S. Yi, "Collaborative unsupervised visual representation learning from decentralized data," in *2021 IEEE/CVF International Conference on Computer Vision*. IEEE, 2021, pp. 4892–4901.
- [12] X. Liao, W. Liu, C. Chen, P. Zhou, F. Yu, H. Zhu, B. Yao, T. Wang, X. Zheng, and Y. Tan, "Rethinking the representation in federated unsupervised learning with non-iid data," in *Proceedings of the IEEE/CVF Conference on Computer Vision and Pattern Recognition*, 2024, pp. 22 841–22 850.
- [13] S. Han, S. Park, F. Wu, S. Kim, C. Wu, X. Xie, and M. Cha, "Fedx: Unsupervised federated learning with cross knowledge distillation," in *European Conference on Computer Vision*. Springer, 2022, pp. 691–707.
- [14] E. S. Lubana, C. I. Tang, F. Kawsar, R. P. Dick, and A. Mathur, "Orchestra: Unsupervised federated learning via globally consistent clustering," in *Proc. International Conference on Machine Learning*, 2022.
- [15] C. Zhang, Y. Xie, T. Chen, W. Mao, and B. Yu, "Prototype similarity distillation for communication-efficient federated unsupervised representation learning," *IEEE Transactions on Knowledge and Data Engineering*, 2024.
- [16] P. Bergmann, S. Löwe, M. Fauser, D. Sattlegger, and C. Steger, "Improving unsupervised defect segmentation by applying structural similarity to autoencoders," in *Proceedings of the 14th International Joint Conference on Computer Vision, Imaging and Computer Graphics Theory and Applications*. SCITEPRESS-Science and Technology Publications, 2019.
- [17] Y. Liang, J. Zhang, S. Zhao, R. Wu, Y. Liu, and S. Pan, "Omni-frequency channel-selection representations for unsupervised anomaly detection," *IEEE Transactions on Image Processing*, 2023.
- [18] S. Dai, Y. Wu, X. Li, and X. Xue, "Generating and reweighting dense contrastive patterns for unsupervised anomaly detection," in *Proceedings of the AAAI Conference on Artificial Intelligence*, vol. 38, no. 2, 2024, pp. 1454–1462.
- [19] T. Lei, S. Chen, B. Wang, Z. Jiang, and N. Zou, "Adapted-moe: Mixture of experts with test-time adaption for anomaly detection," *arXiv preprint arXiv:2409.05611*, 2024.
- [20] S. P. Karimireddy, S. Kale, M. Mohri, S. Reddi, S. Stich, and A. T. Suresh, "Scaffold: Stochastic controlled averaging for federated learning," in *International conference on machine learning*. PMLR, 2020, pp. 5132–5143.
- [21] Y. Zhao, M. Li, L. Lai, N. Suda, D. Civin, and V. Chandra, "Federated learning with non-iid data," *arXiv preprint arXiv:1806.00582*, 2018.
- [22] T. Li, A. K. Sahu, M. Zaheer, M. Sanjabi, A. Talwalkar, and V. Smith, "Federated optimization in heterogeneous networks," *Proceedings of Machine learning and systems*, vol. 2, pp. 429–450, 2020.
- [23] X. Li, M. Jiang, X. Zhang, M. Kamp, and Q. Dou, "Fedbn: Federated learning on non-iid features via local batch normalization," *arXiv preprint arXiv:2102.07623*, 2021.
- [24] M. Jiang, Z. Wang, and Q. Dou, "Harmoff: Harmonizing local and global drifts in federated learning on heterogeneous medical images," in *Proceedings of the AAAI Conference on Artificial Intelligence*, vol. 36, no. 1, 2022, pp. 1087–1095.
- [25] X.-C. Li, Y.-C. Xu, S. Song, B. Li, Y. Li, Y. Shao, and D.-C. Zhan, "Federated learning with position-aware neurons," in *Proceedings of the IEEE/CVF Conference on Computer Vision and Pattern Recognition*, 2022, pp. 10 082–10 091.



- [26] T. Zhou, Y. Yuan, B. Wang, and E. Konukoglu, "Federated feature augmentation and alignment," *IEEE Transactions on Pattern Analysis and Machine Intelligence*, 2024.
- [27] Y. Dai, Z. Chen, J. Li, S. Heinecke, L. Sun, and R. Xu, "Tackling data heterogeneity in federated learning with class prototypes," in *Proceedings of the AAAI Conference on Artificial Intelligence*, vol. 37, no. 6, 2023, pp. 7314–7322.
- [28] A. Fallah, A. Mokhtari, and A. Ozdaglar, "Personalized federated learning with theoretical guarantees: A model-agnostic meta-learning approach," *Advances in neural information processing systems*, vol. 33, pp. 3557–3568, 2020.
- [29] J. Luo and S. Wu, "Adapt to adaptation: Learning personalization for cross-silo federated learning," in *IJCAI: proceedings of the conference*, vol. 2022. NIH Public Access, 2022, p. 2166.
- [30] W. Huang, M. Ye, Z. Shi, H. Li, and B. Du, "Rethinking federated learning with domain shift: A prototype view," in *2023 IEEE/CVF Conference on Computer Vision and Pattern Recognition (CVPR)*. IEEE, 2023, pp. 16312–16322.
- [31] D. C. Nguyen, M. Ding, P. N. Pathirana, A. Seneviratne, and A. Y. Zomaya, "Federated learning for covid-19 detection with generative adversarial networks in edge cloud computing," *IEEE Internet of Things Journal*, vol. 9, no. 12, pp. 10257–10271, 2021.
- [32] Z. Li, Y. Sun, J. Shao, Y. Mao, J. H. Wang, and J. Zhang, "Feature matching data synthesis for non-iid federated learning," *IEEE Transactions on Mobile Computing*, 2024.
- [33] Z. Li, Z. Lin, J. Shao, Y. Mao, and J. Zhang, "Fedcir: Client-invariant representation learning for federated non-iid features," *IEEE Transactions on Mobile Computing*, 2024.
- [34] Y. Tan, G. Long, L. Liu, T. Zhou, Q. Lu, J. Jiang, and C. Zhang, "Fedproto: Federated prototype learning across heterogeneous clients," in *Proceedings of the AAAI Conference on Artificial Intelligence*, vol. 36, no. 8, 2022, pp. 8432–8440.
- [35] J. Zhang, Y. Hua, J. Cao, H. Wang, T. Song, Z. Xue, R. Ma, and H. Guan, "Eliminating domain bias for federated learning in representation space," *Advances in Neural Information Processing Systems*, vol. 36, 2024.
- [36] Z. You, L. Cui, Y. Shen, K. Yang, X. Lu, Y. Zheng, and X. Le, "A unified model for multi-class anomaly detection," *Advances in Neural Information Processing Systems*, vol. 35, pp. 4571–4584, 2022.
- [37] O. R. A. Almanifi, C.-O. Chow, M.-L. Tham, J. H. Chuah, and J. Kanesan, "Communication and computation efficiency in federated learning: A survey," *Internet of Things*, vol. 22, p. 100742, 2023.
- [38] T. Li, A. K. Sahu, A. Talwalkar, and V. Smith, "Federated learning: Challenges, methods, and future directions," *IEEE signal processing magazine*, vol. 37, no. 3, pp. 50–60, 2020.
- [39] T. Li, A. K. Sahu, M. Zaheer, M. Sanjabi, A. Talwalkar, and V. Smith, "Federated optimization in heterogeneous networks," *Proceedings of Machine learning and systems*, vol. 2, pp. 429–450, 2020.
- [40] Z. Yang, W. Bao, D. Yuan, N. H. Tran, and A. Y. Zomaya, "Federated learning with nesterov accelerated gradient," *IEEE Transactions on Parallel and Distributed Systems*, vol. 33, no. 12, pp. 4863–4873, 2022.
- [41] D. Rothchild, A. Panda, E. Ullah, N. Ivkin, I. Stoica, V. Braverman, J. Gonzalez, and R. Arora, "Fetchsgd: Communication-efficient federated learning with sketching," in *International Conference on Machine Learning*. PMLR, 2020, pp. 8253–8265.
- [42] N. Shlezinger, M. Chen, Y. C. Eldar, H. V. Poor, and S. Cui, "Uveqfed: Universal vector quantization for federated learning," *IEEE Transactions on Signal Processing*, vol. 69, pp. 500–514, 2020.
- [43] J. Li, C. Li, J. Fan, and T. Huang, "Online distributed stochastic gradient algorithm for non-convex optimization with compressed communication," *IEEE Transactions on Automatic Control*, 2023.
- [44] J. Xu and H. Wang, "Client selection and bandwidth allocation in wireless federated learning networks: A long-term perspective," *IEEE Transactions on Wireless Communications*, vol. 20, no. 2, pp. 1188–1200, 2020.
- [45] P. Bergmann, S. Löwe, M. Fauser, D. Sattlegger, and C. Steger, "Improving unsupervised defect segmentation by applying structural similarity to autoencoders," *arXiv preprint arXiv:1807.02011*, 2018.
- [46] V. Zavrtnik, M. Kristan, and D. Skočaj, "Draem-a discriminatively trained reconstruction embedding for surface anomaly detection," in *Proceedings of the IEEE/CVF international conference on computer vision*, 2021, pp. 8330–8339.
- [47] J. Jiang, J. Zhu, M. Bilal, Y. Cui, N. Kumar, R. Dou, F. Su, and X. Xu, "Masked swin transformer unet for industrial anomaly detection," *IEEE Transactions on Industrial Informatics*, vol. 19, no. 2, pp. 2200–2209, 2022.
- [48] D. Wu, S. Fan, X. Zhou, L. Yu, Y. Deng, J. Zou, and B. Lin, "Unsupervised anomaly detection via masked diffusion posterior sampling," *arXiv preprint arXiv:2404.17900*, 2024.
- [49] N. Cohen and Y. Hoshen, "Sub-image anomaly detection with deep pyramid correspondences," *arXiv preprint arXiv:2005.02357*, 2020.
- [50] T. Defard, A. Setkov, A. Loesch, and R. Audigier, "Padim: a patch distribution modeling framework for anomaly detection and localization," in *International Conference on Pattern Recognition*. Springer, 2021, pp. 475–489.
- [51] K. Roth, L. Pemula, J. Zepeda, B. Schölkopf, T. Brox, and P. Gehler, "Towards total recall in industrial anomaly detection," in *Proceedings of the IEEE/CVF conference on computer vision and pattern recognition*, 2022, pp. 14318–14328.
- [52] J. Bae, J.-H. Lee, and S. Kim, "Pni: Industrial anomaly detection using position and neighborhood information," in *Proceedings of the IEEE/CVF International Conference on Computer Vision*, 2023, pp. 6373–6383.
- [53] H. Kim, Y. Kwak, M. Jung, J. Shin, Y. Kim, and C. Kim, "Protofl: Unsupervised learning via prototypical distillation," in *Proceedings of the IEEE/CVF International Conference on Computer Vision*, 2023, pp. 6470–6479.
- [54] B. McMahan, E. Moore, D. Ramage, S. Hampson, and B. A. y Arcas, "Communication-efficient learning of deep networks from decentralized data," in *Artificial intelligence and statistics*. PMLR, 2017, pp. 1273–1282.
- [55] Q. Li, Z. Wen, Z. Wu, S. Hu, N. Wang, Y. Li, X. Liu, and B. He, "A survey on federated learning systems: Vision, hype and reality for data privacy and protection," *IEEE Transactions on Knowledge and Data Engineering*, vol. 35, no. 4, pp. 3347–3366, 2021.
- [56] L. Wang, M. Wang, D. Zhang, and H. Fu, "Model barrier: A compact untransferable isolation domain for model intellectual property protection," in *Proceedings of the IEEE/CVF Conference on Computer Vision and Pattern Recognition*, 2023, pp. 20475–20484.
- [57] J. Zhang, Y. Liu, Y. Hua, and J. Cao, "Fedtgp: Trainable global prototypes with adaptive-margin-enhanced contrastive learning for data and model heterogeneity in federated learning," in *Proceedings of the AAAI Conference on Artificial Intelligence*, vol. 38, no. 15, 2024, pp. 16768–16776.
- [58] S. Lee, S. Lee, and B. C. Song, "Cfa: Coupled-hypersphere-based feature adaptation for target-oriented anomaly localization," *IEEE Access*, vol. 10, pp. 78446–78454, 2022.
- [59] K. He, X. Zhang, S. Ren, and J. Sun, "Deep residual learning for image recognition," in *Proceedings of the IEEE conference on computer vision and pattern recognition*, 2016, pp. 770–778.
- [60] J. C. Lee, T. Kim, E. Park, S. S. Woo, and J. H. Ko, "Continuous memory representation for anomaly detection," in *European Conference on Computer Vision*. Springer, 2025, pp. 438–454.
- [61] R. Liu, J. Lehman, P. Molino, F. Petroski Such, E. Frank, A. Sergeev, and J. Yosinski, "An intriguing failing of convolutional neural networks and the coordconv solution," *Advances in neural information processing systems*, vol. 31, 2018.
- [62] X. Glorot and Y. Bengio, "Understanding the difficulty of training deep feedforward neural networks," in *Proceedings of the thirteenth international conference on artificial intelligence and statistics*. JMLR Workshop and Conference Proceedings, 2010, pp. 249–256.
- [63] Y. Tan, G. Long, J. Ma, L. Liu, T. Zhou, and J. Jiang, "Federated learning from pre-trained models: A contrastive learning approach," *Advances in neural information processing systems*, vol. 35, pp. 19332–19344, 2022.
- [64] D. P. Kingma, "Adam: A method for stochastic optimization," *arXiv preprint arXiv:1412.6980*, 2014.
- [65] J. Li, F. Li, L. Zhu, H. Cui, and J. Li, "Prototype-guided knowledge transfer for federated unsupervised cross-modal hashing," in *Proceedings of the 31st ACM International Conference on Multimedia*, 2023, pp. 1013–1022.
- [66] K. Bonawitz, V. Ivanov, B. Kreuter, A. Marcedone, H. B. McMahan, S. Patel, D. Ramage, A. Segal, and K. Seth, "Practical secure aggregation for privacy-preserving machine learning," in *proceedings of the 2017 ACM SIGSAC Conference on Computer and Communications Security*, 2017, pp. 1175–1191.
- [67] S. Zhang, W. Yuan, and H. Yin, "Comprehensive privacy analysis on federated recommender system against attribute inference attacks," *IEEE Transactions on Knowledge and Data Engineering*, 2023.
- [68] U. Baid, S. Ghodasara, S. Mohan, M. Bilello, E. Calabrese, E. Colak, K. Farahani, J. Kalpathy-Cramer, F. C. Kitamura, S. Pati *et al.*, "The rsna-asnr-miccai brats 2021 benchmark on brain tumor segmentation and radiogenomic classification," *arXiv preprint arXiv:2107.02314*, 2021.



- [69] M. Salehi, N. Sadjadi, S. Baselizadeh, M. H. Rohban, and H. R. Rabiee, "Multiresolution knowledge distillation for anomaly detection," in *Proceedings of the IEEE/CVF conference on computer vision and pattern recognition*, 2021, pp. 14 902–14 912.
- [70] D. S. Kermany, M. Goldbaum, W. Cai, C. C. Valentim, H. Liang, S. L. Baxter, A. McKeown, G. Yang, X. Wu, F. Yan *et al.*, "Identifying medical diagnoses and treatable diseases by image-based deep learning," *cell*, vol. 172, no. 5, pp. 1122–1131, 2018.
- [71] X. Wang, Y. Peng, L. Lu, Z. Lu, M. Bagheri, and R. M. Summers, "Chestx-ray8: Hospital-scale chest x-ray database and benchmarks on weakly-supervised classification and localization of common thorax diseases," in *Proceedings of the IEEE conference on computer vision and pattern recognition*, 2017, pp. 2097–2106.
- [72] H. Q. Nguyen, K. Lam, L. T. Le, H. H. Pham, D. Q. Tran, D. B. Nguyen, D. D. Le, C. M. Pham, H. T. Tong, D. H. Dinh *et al.*, "Vindr-cxr: An open dataset of chest x-rays with radiologist's annotations," *Scientific Data*, vol. 9, no. 1, p. 429, 2022.
- [73] Y. Zou, J. Jeong, L. Pemula, D. Zhang, and O. Dabeer, "Spot-the-difference self-supervised pre-training for anomaly detection and segmentation," in *European Conference on Computer Vision*. Springer, 2022, pp. 392–408.
- [74] H. Bai, S. Mou, T. Likhomanenko, R. G. Cinbis, O. Tuzel, P. Huang, J. Shan, J. Shi, and M. Cao, "Vision datasets: A benchmark for vision-based industrial inspection," *arXiv preprint arXiv:2306.07890*, 2023.
- [75] P. Bergmann, M. Fauser, D. Sattlegger, and C. Steger, "Mvtec ad—a comprehensive real-world dataset for unsupervised anomaly detection," in *Proceedings of the IEEE/CVF conference on computer vision and pattern recognition*, 2019, pp. 9592–9600.
- [76] S. Jezek, M. Jonak, R. Burget, P. Dvorak, and M. Skotak, "Deep learning-based defect detection of metal parts: evaluating current methods in complex conditions," in *2021 13th International congress on ultra modern telecommunications and control systems and workshops (ICUMT)*. IEEE, 2021, pp. 66–71.
- [77] X.-C. Li, D.-C. Zhan, Y. Shao, B. Li, and S. Song, "Fedphp: Federated personalization with inherited private models," in *Joint European Conference on Machine Learning and Knowledge Discovery in Databases*. Springer, 2021, pp. 587–602.